JOURNAL OF SOLID STATE CHEMISTRY 53, 64–75 (1984)

The Crystal Structures of the Lithium-Inserted Metal Oxides $Li_{0.5}TiO_2$ Anatase, $LiTi_2O_4$ Spinel, and $Li_2Ti_2O_4$

R. J. CAVA, D. W. MURPHY, AND S. ZAHURAK

Bell Laboratories, 600 Mountain Avenue, Murray Hill, New Jersey 07974

AND A. SANTORO AND R. S. ROTH

National Bureau of Standards, Washington, D.C. 20234

Received October 24, 1983; in revised form January 3, 1984

The crystal structures of three lithium titanates by neutron diffraction powder profile analysis were determined. The tetragonal anatase form of TiO_2 becomes orthorhombic on ambient-temperature lithium insertion to $Li_{0.5}TiO_2$ due to the formation of Ti–Ti bonds. The lithium partially occupies the highly distorted octahedral interstices in the anatase framework in fivefold-coordination with oxygen. Cubic $LiTi_2O_4$ formed by heating $Li_{0.5}TiO_2$ anatase has a normal spinel structure with Li in the tetrahedral sites. In $Li_2Ti_2O_4$ formed by reacting $LiTi_2O_4$ spinel with *n*-BuLi at ambient temperature, the titanium remains in the spinel positions but the lithium is displaced, filling all the available octahedral sites.

Transition metal oxides with tunnel or framework structures have been investigated intensively as hosts for lithium insertion at ambient temperature. The study of TiO_2 based compounds affords a variety of such structures of related chemistry with different host geometries. Both the Brookite and Rutile forms of TiO_2 insert only small amounts of Li either electrochemically or from *n*-BuLi, whereas the anatase and TiO_2 (B) forms react extensively, with stoichiometries up to about 0.7 Li/Ti (*1–4*). For anatase, the originally tetragonal host structure becomes orthorhombic on Li insertion. The product $Li_{0.5}TiO_2$ is obtained on reaction of *n*-BuLi with anatase under mild conditions, and on heating to 450–500°C transforms from the orthorhombic phase to a cubic spinel phase with a crystallographic unit cell and electrical properties (superconducting phase transition at about ~12–13 K) identical to those of the $LiTi_2O_4$ phase synthesized at high temperatures (*5*). Reaction of this cubic phase $LiTi_2O_4$ with *n*-BuLi results in the accommodation of additional lithium, to a stoichiometry of $Li_2Ti_2O_4$, with a small contraction of the cubic crystallographic unit cell dimension.

In this report we elucidate the results of structural studies of the compounds $Li_{0.5}TiO_2$ (anatase), the $LiTi_2O_4$ cubic phase prepared by heating that compound above 450°C, and the $Li_2Ti_2O_4$ product obtained by lithiation of the cubic $LiTi_2O_4$ phase at ambient temperature. The structures of all 3 phases were determined by neutron diffraction powder profile analysis (NDPPA). Detailed structural study is otherwise not possible on such materials, because single crystals are not available.

0022-4596/84 $3.00

We have found the inserted Li ions to partially occupy the octahedral interstices in the highly distorted cubic close-packed (ccp) oxygen array in anatase TiO_2. Within those interstices, their coordination is closer to five- than to sixfold. The tetragonal to orthorhombic distortion is due to the formation of zigzag chains of Ti–Ti bonds, whose presence is suggested by the nonmetallic resistivity of the Li-anatase (*3*), attributable to localized electrons. On heating above 450°C, the compound becomes electrically conductive, the structure changes irreversibly to spinel type $LiTi_2O_4$ with the coordination of Li changing from five- to fourfold, and the anion array distorted only slightly from ideal ccp. The $LiTi_2O_4$ phase formed at elevated temperatures also has the spinel structure, although a detailed crystallographic study has not yet been reported. On further lithiation of the $LiTi_2O_4$ phase to $Li_2Ti_2O_4$, the lithium is completely displaced from the tetrahedral sites and fills the octahedral sites, while the titanium positions are unchanged. The structure of $Li_2Ti_2O_4$ may be thought of as a new ordered rock salt type, with the ccp oxygen array insignificantly distorted from ideal.

Experimental

Neutron diffraction measurements were performed on the high-resolution five-counter powder diffractometer at the NBS Reactor, with neutrons of wavelength 1.5416(3) Å. The experimental conditions used to collect the data are presented in Table I. The powder profile refinement was performed using the Rietveld program (*7*) adapted to the 5-detector diffractometer design and modified to allow the refinement of background intensity (*8*). The program has been further modified to describe non-Gaussian profiles with the Pearson Type VII distribution, which allows the lineshape to be varied continuously from Gaussian to Lorentzian by changing one additional profile parameter. This method, described in detail elsewhere (*9*) was critical in the refinements of the structures. For $Li_{0.5}TiO_2$ anatase and $LiTi_2O_4$ spinel the profile was best fit for peak shapes described by the Pearson Type VII distribution with $2m = 8$, a modified Gaussian shape. For $Li_2Ti_2O_4$, a more Lorentzian $2m = 5$ was the best fit to the peak shapes.

TABLE I

EXPERIMENTAL CONDITIONS USED TO COLLECT THE NEUTRON POWDER INTENSITY DATA FOR LITHIUM TITANIUM OXIDES

Monochromatic beam	Reflection 220 of a Cu monochromator	
Wavelength	1.5416(3) Å	
Horizontal divergences	(a) In-pile collimator	10′ arc
	(b) Monochromatic beam collimator	20′ arc
	(c) Diffracted beam collimator	10′ arc
Monochromator spread	~15′ arc	
Sample container	Vanadium can ~10 mm in diameter	
Angular ranges scanned by each detector	10–40, 30–60, 50–80, 70–100, 90–120	
Angular step	0.05°	

The neutron scattering amplitudes employed were $b(\mathrm{Li}) = -0.214$, $b(\mathrm{Ti}) = -0.344$, and $b(\mathrm{O}) = 0.58$ ($\times 10^{-12}$ cm) (*10*). Approximate values of the background parameters were obtained at positions in the pattern free from diffraction effects, and initial unit cell parameters were obtained by least-squares fits to several low angle lines in powder X-ray diffraction patterns for all compounds. In the refinement of the structural models, all structural, lattice, and profile parameters were refined simultaneously. Refinements were terminated when in two successive cycles the factor R_w

TABLE II

THE STRUCTURE OF $Li_{0.5}TiO_2$ (ANATASE TYPE)

	Crystallographic unit cell		
	a	*b*	*c*
$Li_{0.5}TiO_2$	3.8082(1)	4.0768(1)	9.0526(4)
Anatase	3.784(1)	3.784(1)	9.515(2)

$Li_{0.5}TiO_2$
Space group: *Imma*, $z = 4$

Atom		Position			Thermal parameter B, Å^2
		x	*y*	*z*	
Ti	4*e*	0	$\frac{1}{4}$	.8871(5)	.91(7)
O1	4*e*	0	$\frac{1}{4}$	.1030(2)	.71(5)
O2	4*e*	0	$\frac{1}{4}$	.6521(2)	.75(5)
Li[a]	4*e*	0	$\frac{1}{4}$	.343(2)	.59(3)

$R_N = 6.71\%$ $R_p = 6.59\%$ $R_w = 8.81\%$ $R_E = 6.37\%$

Anatase TiO_2 in same space group (*I1*):

Atom	Position	*x*	*y*	*z*
Ti	4e	0	$\frac{1}{4}$	.875
O	4e	0	$\frac{1}{4}$	.082
O	4e	0	$\frac{1}{4}$	.668

$$R_N = \frac{\Sigma|I(\text{obs}) - I(\text{calc})|}{\Sigma I(\text{obs})}$$

$$R_p = \frac{\Sigma|y(\text{obs}) - y(\text{calc})|}{\Sigma y(\text{obs})}$$

$$R_w = \left\{\frac{\Sigma w[y(\text{obs}) - y(\text{calc})]^2}{\Sigma w[y(\text{obs})]^2}\right\}^{1/2}$$

$$R_E = \left\{\frac{N - P + C}{\Sigma w[y(\text{obs})]^2}\right\}^{1/2}$$

where N = number of independent observations, P = number of parameters, C = number of constraints, y = counts at angle 2θ, I = integrated Bragg intensities, and w = weights

[a] Two Li/Cell are disordered over the 4 equivalent 4*e* positions.

(see Table II) varied by less than one part in a thousand. In the final refinements, 15 profile parameters were varied for each compound, 5 structural parameters were refined for the cubic phases, and 11 for orthorhombic $Li_{0.5}TiO_2$ anatase (including lattice parameters).

Results

$Li_{0.5}TiO_2$ (Anatase)

The space group of anatase is $I4_1/amd$ (No. 141). The 4 formula units/crystallographic unit cell are distributed such that Ti occupy 4 equivalent sites of fixed position

(4*a*, *000*) and the O occupy 8 equivalent sites with 1 variable parameter (8*e*, *00z*, $z = 0.2081$) (*11*). On lithiation, tetragonal symmetry is broken, and the unit cell becomes orthorhombic, with the two formerly equivalently a_0 directions becoming different in length by about 7% and the *c* axis shrinking by about 5%. The cell parameters are presented in Table II. Inspection of both the powder X-ray diffraction and neutron diffraction patterns of $Li_{0.5}TiO_2$ indicates that the anatase unit cell has maintained its body centering on lithium insertion, and comparison of the relative intensities of the powder diffraction lines for $Li_{0.5}TiO_2$ and anatase indicates that the TiO_2 host has not been greatly distorted on lithium insertion. Consideration of the orthorhombic space groups indicates that only a few are consistent with positions that would be obtained from those of the atoms in tetragonal TiO_2 with minor distortion. These space groups are *Imm*2, *Imma*, and *Ima*2. The approximate coordinates of the Ti and O atoms in *Imm*2 are obtained from the coordinates in tetragonal anatase by a simple one-to-one correspondence of the $I4_1/amd$ 4*a* (Ti) positions and 8*e* (O) positions with the 2*a* and 2*b* positions in *Imm*2. The decrease in symmetry from tetragonal to orthorhombic in this case results in two inequivalent Ti positions (thus allowing the possibility of localization of Ti^{4+}, Ti^{3+} ions) and four inequivalent oxygen positions. To obtain approximate positional coordinates in *Imma* and *Ima*2, the atom coordinates in anatase must first be transformed from those in the first setting of $I4_1/amd$ to a coordinate system where the center of symmetry is the origin of the space group by adding the vector (0.025, −0.125). Again, a simple one to one correspondence of the Ti and O positions in anatase to positions in *Imma* and *Ima*2 can be found. In *Imma*, the 4*e* positions correspond to the 4*a* positions for Ti in $I4_1/amd$, and the 8*e* positions in $I4_1/amd$, become two inequivalent sets of 4*e* positions, allowing the distinction of two independent sets of oxygen atoms. The possible atomic positions in *Ima*2 are exactly equivalent to those for *Imma* except that each set of atoms is allowed one additional positional degree of freedom.

Initial refinements of the structure were in space group *Imm*2 and indicated that the Ti and O atoms were indeed close to those positions predicted by a direct one-to-one correspondence to the positions in anatase. Difference Fourier synthesis based on the observed and calculated structure factors extracted from the profile fit indicated that the Li ions were located in the vacant octahedral interstices in the distorted ccp oxygen array. In *Imm*2 there are two symmetrically inequivalent Li positions, and refinement of the occupancies (two Li/cell are distributed over four total sites) indicated that they were occupied with equal probability. Refinement in *Imm*2 proceeded to the agreement factors $R_N = 8.88$, $R_p = 7.16$, $R_w = 9.55$ with $R_E = 6.37$. (The agreement factors based on Bragg intensities, profile, and weighted profile fits, and that expected based on statistics alone, respectively.) There are two symmetrically independent Ti and Li positions and four symmetrically independent O positions in this space group. Inspection of the atomic coordinates for each atom type indicated that the refined positions fell into groups of two sets of multiplicity two which, within several standard deviations, were equivalent to the multiplicity four positions of the atoms when described in space group *Imma*. Therefore the higher symmetry space group was indicated.

Refinement in space group *Imma* proceeded smoothly to better agreement factors than obtained in *Imm*2, $R_N = 6.71$, $R_p = 6.59$, $R_2 = 8.81$, $R_E = 6.37$, indicating that this space group was indeed correct. The final atomic coordinates are presented in Table II. In *Imma* all Ti atoms are symmetrically equivalent, as are all Li atoms,

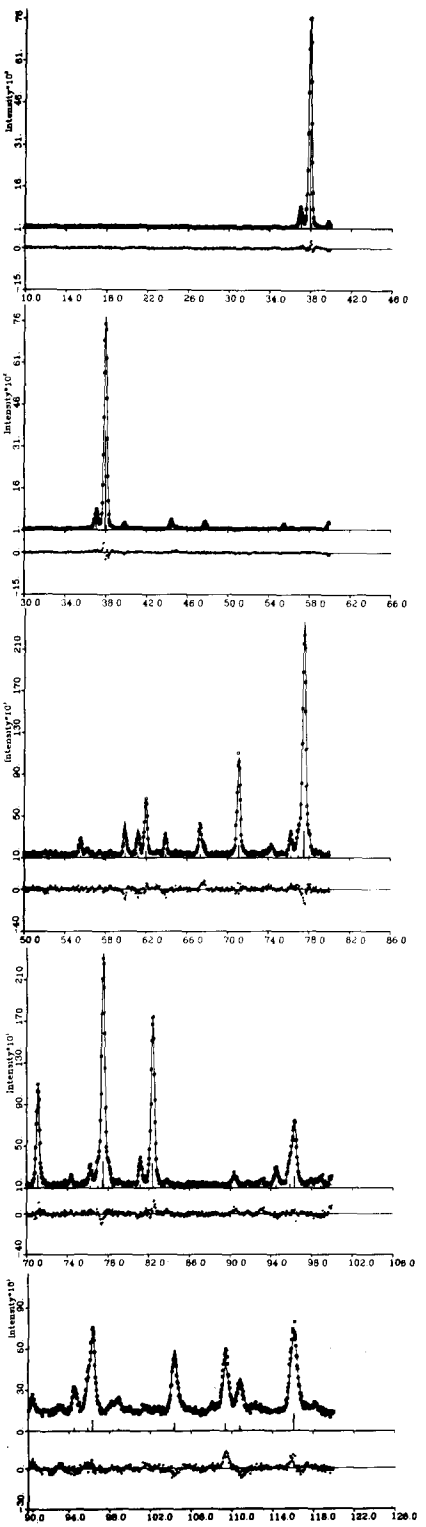

and there are two sets of symmetry equivalent oxygen atoms. The two Li/cell are randomly distributed over the four available octahedral interstices. The relatively small distortion of the host structure on Li insertion can be seen by comparing the Ti and O positions in $Li_{0.5}TiO_2$ with those for TiO_2 anatase transposed to the same coordinate system (Table II). Finally, refinements in *Ima*2 involving the addition of one positional degree of freedom perpendicular to *c* for each of the sets of atomic positions in *Imma* and did not result in significant displacements of the atoms from their *Imma* positions, and thus the coordinates presented in Table II are the final structural parameters for $Li_{0.5}TiO_2$ anatase. Comparison of the observed and calculated neutron diffraction powder profiles is presented in Fig. 1.

The structure of $Li_{0.5}TiO_2$ is shown in Fig. 2, in which the TiO_6 octahedra of the anatase framework are emphasized by solid and dotted lines. The anatase framework has been distorted very little by the insertion of the lithium. The distortions from regularity of the TiO_6 octahedra are actually smaller for $Li_{0.5}TiO_2$ than for anatase. For both structures, the oxygen array is significantly distorted from the ideal cubic close-packing arrangement. Bond lengths and angles for the TiO_6 coordination polyhedron are presented in Table III. Comparison of the Ti–O distances to those in anatase, 1.934(×4) and 1.980(×2) Å (*11*), indicates a general expansion and a larger range of distances in $Li_{0.5}TiO_2$. The O–Ti–O bond angles are more regular than those in anatase (101.9° (*11*)), as are the O–O distances (2.47–3.04 Å in anatase (*11*)). There are two sets of Ti–Ti distances, 2.887, and

FIG. 1. Observed and calculated neutron diffraction powder pattern for $Li_{0.5}TiO_2$, anatase form. Below the observed and calculated patterns for each counter, plotted on the same scale, is the difference between observed and calculated intensities.

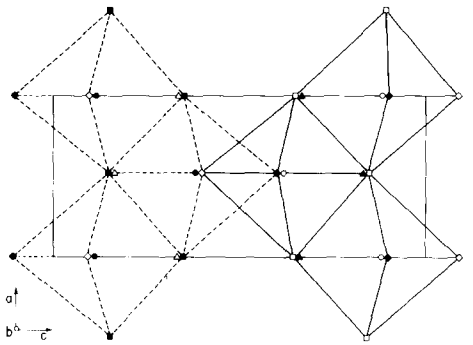

FIG. 2. The structure of $Li_{0.5}TiO_2$, anatase form, c axis horizontal, a axis vertical, b axis out of the page. Open and closed symbols are at $y = \frac{1}{4}$ and $y = \frac{3}{4}$, respectively: △ = Li, ○ = Ti, ◇ = O1, □ = O2. The anatase TiO_2 framework has been accentuated by outlining the TiO_6 octahedra.

3.128 Å, which occur so as to form zigzag Ti–Ti bonded chains along the b direction.

The vacant "octahedral" interstices in anatase are quite irregular, and the lithium in $Li_{0.5}TiO_2$ is actually five-coordinated to the oxygen of the framework. Five oxygen atoms can be found at distances of 1.97–2.17 Å, with one oxygen beyond the first-coordination shell at 2.80 Å (Table III). The fivefold Li–O coordination in $Li_{0.5}TiO_2$ is quite similar to the fivefold-coordination for Li in the insertion compound $Li_2FeV_3O_8$ (*12*). The inserted Li increases the regularity of the octahedral interstice somewhat. The Li–O coordination polyhedron is presented in Fig. 3A, the Li ion is situated in the available interstice in a manner that allows five distances to be approximately 2 Å.

$LiTi_2O_4$ Spinel

Structural refinement for the $LiTi_2O_4$ cubic phase obtained by heating $Li_{0.5}TiO_2$ anatase above 500°C was straightforward. Initial coordinates for all atoms were taken as those of an ideal spinel structure, space group $Fd3m$, and initial lattice parameter a_0 taken as that previously reported for the phase of same stoichiometry synthesized at

TABLE III

BOND LENGTHS AND ANGLES FOR $Li_{0.5}TiO_2$ (ANATASE FORM)

I. Lithium coordination polyhedron	
Li–O1(×2)	1.966(5)
Li–O2(×2)	2.039(5)
Li–O1	2.17(2)
Li–O2	2.80(2)
O1–Li–O2(×4)	89.7(1)
O1–Li–O2(×2)	75.6(5)
O1–Li–O1(×2)	104.4(5)
O1–Li–O1	151.2(10)
O2–Li–O2	177.5(10)
O1–Li–O2	180
O1–O1(×2)	3.273(3)
O1–O2(×2)	3.012(2)
O1–O2(×2)	2.993(2)
O1–O2(×4)	2.825(1)
O2–O2(×2)	3.427(3)
II. Titanium coordination polyhedron	
Ti–O1(×2)	2.040(1)
Ti–O2(×2)	1.937(1)
Ti–O1	1.955(5)
Ti–O2	2.127(5)
O1–Ti–O2(×4)	90.46(2)
O1–Ti–O2(×2)	92.5(1)
O1–Ti–O1(×2)	87.5(1)
O2–Ti–O2(×2)	79.4(1)
O2–Ti–O2	158.9(3)
O1–Ti–O1	175.0(3)
O1–Ti–O2	180
O1–O1(×2)	2.763(2)
O1–O2(×2)	3.012(2)
O1–O2(×4)	2.825(1)
O1–O2(×2)	2.993(2)
O2–O2(×2)	2.601(3)
III. Metal–Metal Distances	
TI–Ti(×2)	2.887(6)
Ti–Ti(×2)	3.128(7)
Li–Li(×2)	2.54(2)
Li–Li(×2)	3.50(1)
Li–Li(×4)	2.818(3)
Li–Ti(×2)	2.91(1)
Li–Ti(×2)	3.10(1)

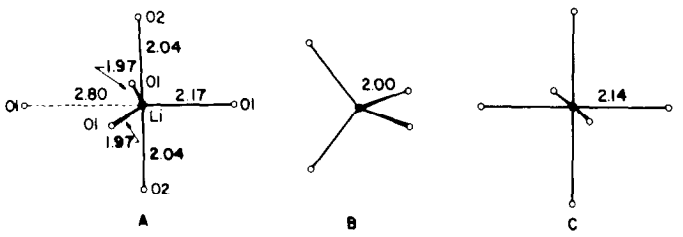

FIG. 3. Comparison of lithium coordination geometries. (A) Five-coordinate Li–O geometry in $Li_{0.5}TiO_2$, anatase, (B) tetrahedrally coordinated Li in $LiTi_2O_4$, and (C) octahedrally coordinated Li in $Li_2Ti_2O_4$.

high temperatures (*5*). Taking the origin of *Fd3m* at the center of symmetry, the Li fully occupy (in an ordered array) the tetrahedral interstices site 8*a*, $(\frac{1}{8}, \frac{1}{8}, \frac{1}{8})$ in the ccp oxygen array, the Ti are in octahedral sites 16*d* $(\frac{1}{2}, \frac{1}{2}, \frac{1}{2})$, and the O are in sites 32*e* (*x*, *x*, *x*) with a variable positional parameter *x* approximately equal to $\frac{1}{4}$. The final structural parameters are presented in Table IV. The agreement factors for Bragg intensities, profile, and weighted profile fits, compared to that expected from statistics alone, are indicative of the excellent fit of the data to the spinel structure. The difference Fourier map employing the observed and calculated structure factors extracted from the profile fit indicated no significant anomalies. Observed and calculated neutron diffraction powder profiles are shown in Fig. 4. The structure of $LiTi_2O_4$ spinel is presented in Fig. 5.

TABLE IV

THE STRUCTURES OF $LiTi_2O_4$ (SPINEL) AND $Li_2Ti_2O_4$

		Space Group *Fd3m* $LiTi_2O_4$	$Li_2Ti_2O_4$
	a_0, Å	8.4033(1)	8.3756(1)
Ti			
	Position	16*d* (0.5, 0.5, 0.5)	16*d* (0.5, 0.5, 0.5)
	B, Å^2	0.46(3)	0.2(1)
Li			
	Position	8*a* (0.125, 0.125, 0.125)	16*c* (0, 0, 0)
	B, Å^2	2.0(1)	2.0(2)
O			
	Position	32*e* (*x*, *x*, *x*)	32*e* (*x*, *x*, *x*)
		x = .26257(5)	x = .2552(2)
	B, Å^2	0.60(2)	0.53(3)
		Agreement factors	
	R_N (%)	5.74	4.06
	R_p (%)	6.78	7.72
	R_w (%)	9.16	10.16
	R_E (%)	5.38	6.22

The transition at 500°C from the $Li_{0.5}TiO_2$ anatase-based structure to that of $LiTi_2O_4$ spinel involves major structural reorganization. Although the oxygen array is nominally cubic close-packed in both cases, that of $Li_{0.5}TiO_2$ is severely distorted whereas that of $LiTi_2O_4$ is nearly ideal; as seen in the oxygen positional parameter of 0.263 compared to the ideal 0.250. During the phase transition the Ti atoms remain octahedrally coordinated but undergo major spatial rearrangement. The lithium ion coordination changes from five- to fourfold with oxygen, and they become long-range ordered. Bond lengths and angles for $LiTi_2O_4$ are presented in Table V. The lithium coordination is that of an ideal tetrahedron, with equal Li–O bond distances and O–Li–O bond angles of 109.47°. The 2.00-Å Li–O bond distance is in good agreement with those found for Li–O in other oxides. The LiO_4 tetrahedron is shown in Fig. 3B. The TiO_6 octahedron is significantly more regular than it is in $Li_{0.5}TiO_2$ anatase, but is still somewhat distorted from the ideal, with equal Ti–O bond distances, but O–Ti–O angles (83.8 and 96.2°) which deviate from the ideal 90°.

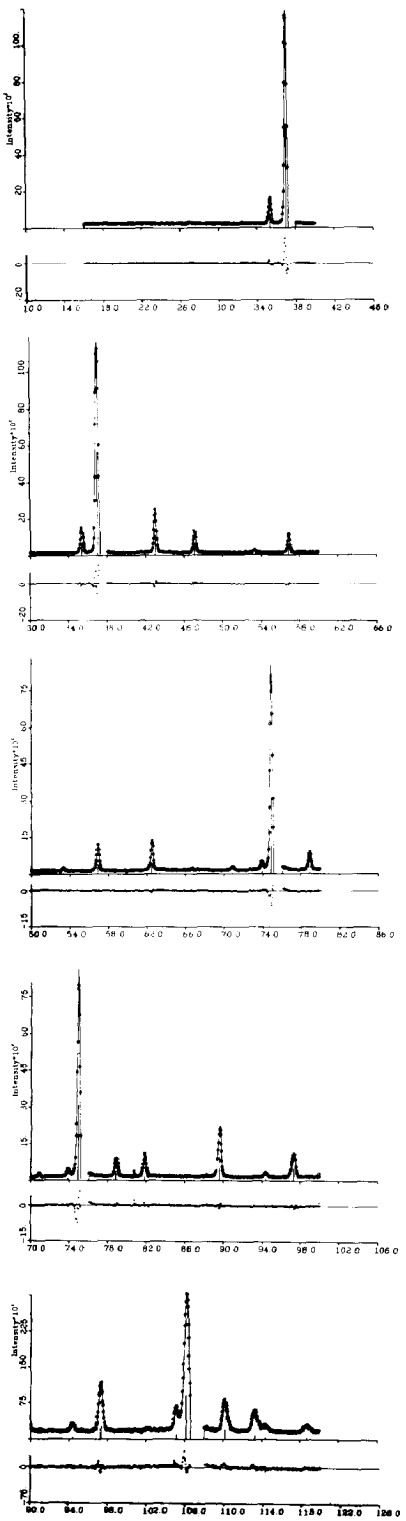

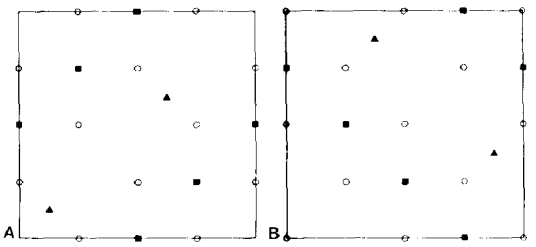

FIG. 5. The structure of $LiTi_2O_4$ spinel in the (*ool*) plane. (A) Oxygen, ○, and Ti, ■, at $z = 0$; ▲ = Li at $z = \frac{1}{8}$. (B) Oxygen, ○, and Ti, ■, at $z = \frac{1}{4}$, and Li, ▲, at $z = \frac{3}{8}$. Other levels related by face centering.

The Ti–O bond distance of 2.001 Å is not significantly different from the average Ti–O distance in $Li_{0.5}TiO_2$ anatase, 2.006 Å. Each Ti in the spinel phase has six equidistant Ti neighbors at distances of 2.97 Å, a value intermediate to the bonding and nonbonding distances found in $Li_{0.5}TiO_2$ anatase.

$Li_2Ti_2O_4$

Refinement of the structure of the $Li_2Ti_2O_4$ phase obtained by room-temperature insertion of Li into $LiTi_2O_4$ also proceeded in a straightforward manner. Initial coordinates for Ti and O atoms were taken as those determined for $LiTi_2O_4$ spinel. The positions, in $Fd3m$, origin at center of symmetry, are Ti, 16*d* ($\frac{1}{2}$, $\frac{1}{2}$, $\frac{1}{2}$), and O, 32*e* (*x*, *x*, *x*), *x* approximately 0.25. Difference Fourier synthesis employing the observed and calculated Bragg intensities extracted from the profile fit indicated that the Li fully occupied the 16*c* (*0*, *0*, *0*) positions, the octahedral interstices. Structural parameters for the final model of $Li_2Ti_2O_4$ are presented in Table IV. The structure is an ordered rock salt type, with Li and Ti occupying all the octahedral interstices in a nearly ideal ($x = 0.255$ for O, 0.25 ideal value) cubic

FIG. 4. Observed and calculated neutron diffraction powder patterns for $LiTi_2O_4$. Below the observed and calculated patterns for each counter, plotted on the same scale, is the difference between the observed and calculated intensity.

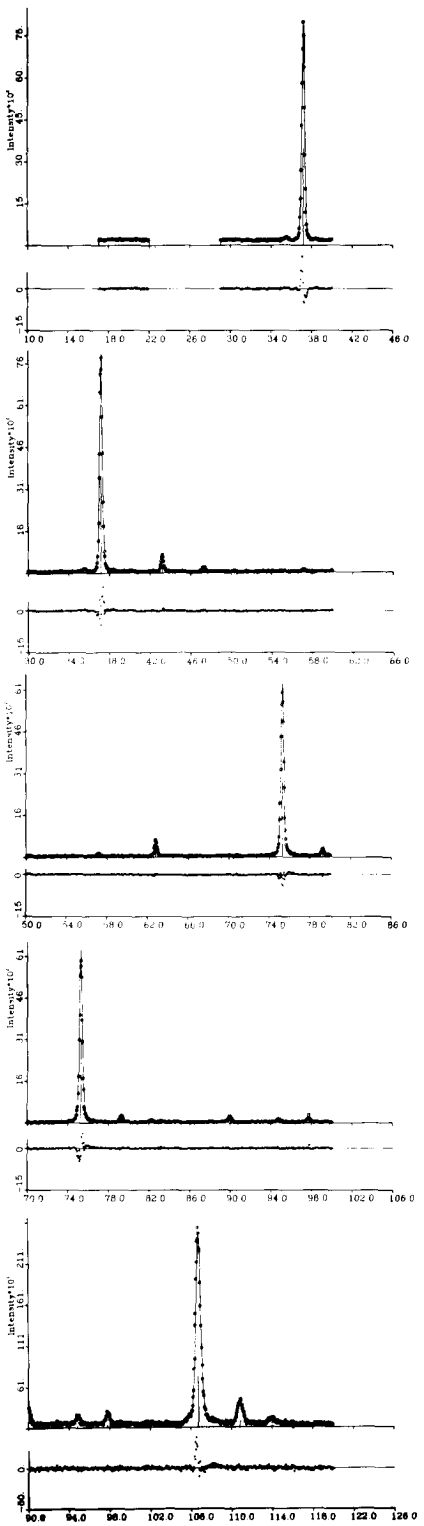

TABLE V

BOND LENGTHS AND ANGLES $LiTi_2O_4$ (SPINEL) AND $Li_2Ti_2O_4$

	Distance or angle (Å or degrees)
$LiTi_2O_4$	
I. Lithium–oxygen tetrahedron	
Li–O(×4)	2.002(1)
O–Li–O(×6)	109.47(2)
O–O(×6)	3.270(1)
II. Titanium–oxygen octahedron	
Ti–O(×6)	2.001(1)
O–Ti–O(×6)	83.80(2)
(×6)	96.20(2)
(×3)	180
O–O(×6)	2.979(1)
(×6)	2.672(1)
III. Metal–metal	
Li–Li	3.639(1)
Ti–Ti	2.971(1)
Li–Ti	3.484(1)
$Li_2Ti_2O_4$	
I. Lithium–oxygen octahedron	
Li–O(×6)	2.138(2)
O–Li–O(×6)	92.31(6)
(×6)	87.54(7)
(×3)	180
O–O(×6)	2.963(1)
(×6)	2.838(3)
II. Titanium–oxygen octahedron	
Ti–O(×6)	2.051(2)
O–Ti–O(×6)	92.46(7)
(×6)	87.54(7)
(×3)	180
O–O(×6)	2.963(1)
(×6)	2.838(3)
III. Metal–metal	
Li–Li	2.961(1)
Ti–Ti	2.961(1)
Li–Ti	2.961(1)

close-packed oxygen array. The agreement factors presented in Table IV indicate an excellent fit of the structural model to the powder neutron diffraction data, and a dif-

FIG. 6. Observed and calculated neutron diffraction patterns for $Li_2Ti_2O_4$. Below the observed and calculated patterns for each counter, plotted on the same scale, is the difference between the observed and calculated intensity.

ference Fourier synthesis based on observed and calculated structure factors showed no significant features. Observed and calculated neutron diffraction powder profiles are presented in Fig. 6, and a representation of the final structural model in Fig. 7.

The Ti and O positions in $LiTi_2O_4$ are virtually unchanged on the insertion of Li to form $Li_2Ti_2O_4$, with the volume of the unit cell decreasing by 1% with the additional Li ion per formula unit. The major difference occurs in the coordination of Li, which changes from tetrahedral to octahedral. The octahedral Li coordination minimizes Li–Li interactions and makes all Li atoms equidistant. Bond lengths and angles for $Li_2Ti_2O_4$ are presented in Table V. Both the LiO_6 and TiO_6 octahedra are of nearly ideal geometry, each with six equal M–O distances and O–M–O angles very close to 90°. The Li–O distance is larger (2.14 Å) in the octahedral configuration than in the tetrahedral (2.00 Å) configuration, as expected. The Li^+O_6 octahedron is slightly larger than the $Ti^{3+}O_6$ octahedron, and is shown in Fig. 3C. The Ti–Ti distances have not changed significantly on insertion of Li Ti_2O_4 to $Li_2Ti_2O_4$, although the Li–Li and Li–Ti separations have decreased, due to the doubling of the number of Li atoms per unit cell. The oxygen array is even closer to ideal ccp in $Li_2Ti_2O_4$ than in $LiTi_2O_4$, with a variation of O–O distances of only 0.24 Å in the former, compared to 0.60 Å in the latter.

Discussion and Conclusions

The lithium titanium oxides formed on the basis of lithium insertion in anatase TiO_2 display interesting physical and structural characteristics. The structural studies of $Li_{0.5}TiO_2$ anatase find the inserted Li ions to occupy $\frac{1}{2}$ of the available "octahedral" interstices, in a 5-coordinate Li–O polyhedron, in the distorted ccp TiO_2 anatase host structure.

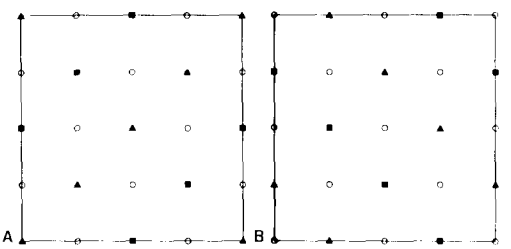

FIG. 7. The structure of the ordered rock salt $Li_2Ti_2O_4$ phase in the (*ool*) plane. Oxygen, ○; Ti, ■; and Li, ▲. (A) $z = 0$. (B) $z = \frac{1}{4}$. Other levels related by face centering.

Although the electron counts for $Li_{0.5}TiO_2$ (anatase) and $LiTi_2O_4$ (spinel) are equivalent, the former has very low electrical conductivity and magnetic susceptibility, whereas the latter is a high T_c superconductor (*3, 5*). The structure of TiO_2 anatase is such that Ti–Ti distances are 3.039 Å, a nonbonded distance. In $Li_{0.5}TiO_2$ the Ti–Ti distances have become differentiated (Table III) to sets of long (3.128 Å) and short (2.887 Å) distances, indicating the probable localization of the 0.5 electron donated by the inserted Li in Ti–Ti bonds. The short Ti–Ti separation is shorter than the separation in $LiTi_2O_4$ spinel (Table V), where all Ti–Ti neighbors are 2.97-Å distant. Comparison of the Ti–Ti separations in $Li_{0.5}TiO_2$ to those found for Ti_3O_5 (*13*), which range from 2.61 to 3.17 Å across shared octahedral edges, indicates the short 2.87-Å separation in $Li_{0.5}TiO_2$ to be characteristic of an intermediate strength Ti–Ti bond. The bonded Ti atoms in $Li_{0.5}TiO_2$ form zigzag chains within edge-shared octahedra running parallel to the *b* axis. Parallel to the *a* axis are only the long (3.13 Å) distances. The existence of the metal–metal bonds exclusively along *b* thus explains the reduction in symmetry from tetragonal to orthorhombic on Li insertion, and the differentiation of the length of the *a* and *b* unit cell dimensions. All Ti atoms are equivalent and involved in two bonds, which are thus formally quarter electron bonds. The inter-

mediate Ti–Ti separation is consistent with that bond strength.

Chemical and electrochemical insertion experiments have found that Li can be inserted into anatase to a maximum stoichiometry of $Li_{0.7}TiO_2$. The structural study of $Li_{0.5}TiO_2$ has found the Li to partially occupy the "octahedral" interstices in a disordered manner, in a five-coordinate polyhedron. Complete filling of the available sites would result in a stoichiometry $LiTiO_2$. The 0.7 Li/Ti stoichiometry limit is therefore not imposed by the availability of interstitial sites in the TiO_2 host, but is apparently due to Li–Li repulsive interactions across an edge shared by neighboring LiO_5 polyhedron, where the separation would be 2.54 Å for neighboring polyhedra simultaneously occupied. The significant distortion in the TiO_2 host array results in an interstitial site geometry where the potential Li sites have sets of short (2.54 Å) and long (3.50 Å) Li–Li separations. In this regard, comparison of the structure of $Li_{0.5}TiO_2$ to that of the tetragonal phase of $LiFeO_2$ synthesized below 650°C, is of interest (*14*). The crystallographic unit cell parameters, 4.048, 4.048, and 8.737 Å, are quite comparable to those of $Li_{0.5}TiO_2$ (3.808, 4.077, and 9.053 Å), and the tetragonal symmetry is that of anatase, as there are no metal–metal bonds. The Li and Fe coordinations are nearly regular octahedra, with the same cation ordering scheme as in $Li_{0.5}TiO_2$, and the oxygen array is much closer to that of ideal ccp. For this compound, with only a slightly larger unit cell volume than that of $Li_{0.5}TiO_2$, the Li–Li separations are all equal at approximately 2.98 Å. Thus for an FeO_2 structure of anatase-like geometry, one Li per Fe can be accommodated in the array of octahedral interstitial sites, due to their relatively large separation; which can be attributed, in turn, to the regularity of the Fe and O array. In Li_xTiO_2, the severe distortion of the interstitial site geometry does not allow the accommodation of Li in sites with large Li–Li separations, and a limit of $x = 0.7$ is reached when the Li–Li repulsive interactions become very strong. These repulsive interactions become stronger in two ways as x is increased, due both to the increase in the concentration of Li, which increases the number of Li–Li neighbors at 2.54 Å, and to the increasing distortion of the TiO_2 array due to the strengthening of the Ti–Ti bonding as more electrons from the inserted Li ions are donated to the bond.

The transformation from $Li_{0.5}TiO_2$ anatase to $LiTi_2O_4$ spinel at 450°C is apparently one of extensive crystallographic strain relief: the highly distorted $Li_{0.5}TiO_2$ anatase structure becomes a nearly ideal ccp spinel, with quite regular coordination polyhedra. Previous studies have found this spinel phase to display the same superconducting properties as the $LiTi_2O_4$ phase prepared by conventional high temperature synthesis techniques, and therefore the details of the structural model for $LiTi_2O_4$ spinel developed here are likely to hold true for the compound synthesized at high temperature. $LiTi_2O_4$ spinel can further react with *n*-BuLi at room temperature to form $Li_2Ti_2O_4$, a 1 : 1 Li : Ti ratio unattainable in the anatase form. This ordered rock salt phase is of nearly ideal dimension, indicating a good balance of the electrostatic forces. In order to accommodate the additional lithium, the tetrahedrally coordinated lithium has been displaced to occupy octahedral sites, with an accompanying sharp drop in the emf of an electrochemical cell (vs Li metal) (*6*). The equilibrium high temperature phase at this composition, $LiTiO_2$, is of the rock salt type, with Li and Ti randomly distributed among the octahedral sites of the fcc oxygen array. The nearly exact equivalence of the LiO_6 and TiO_6 octahedra in the ordered compound $Li_2Ti_2O_4$ studied here suggests that the increased entropy of the disordered phase is the main reason for its preferred thermodynamic sta-

bility. Li displays four-, five-, and six-fold coordination with oxygen in this series of compounds. Studies of the insertion chemistry and structures of lithium–titanium oxides have been fruitful in developing an understanding of Li insertion in close-packed oxide structures, which has been discussed in detail in a previous publication (*6*).

References

1. F. Bonino, M. Lazzari, and L. P. Bicelli, *J. Electrochem. Soc. Proc.* **81-4,** 255 (1981).
2. M. S. Whittingham and M. B. Dines, *J. Electrochem. Soc.* **124,** 1388 (1977).
3. D. W. Murphy, M. Greenblatt, S. M. Zahurak, R. J. Cava, J. V. Waszczak, G. W. Hull, Jr., and R. S. Hutton, *Rev. Chim. Miner.* **19,** 441 (1982).
4. R. Marchand, L. Brohan, and M. Tournoux, *Mater. Res. Bull.* **15,** 1129 (1980).
5. D. C. Johnson, H. Prakash, W. H. Zachariasen, and R. Wiswanathan, *Mater. Res. Bull.* **8,** 777 (1973).
6. D. W. Murphy, R. J. Cava, S. M. Zahurak, and A. Santoro, *Solid State Ionics* **9/10** 413 (1983).
7. H. M. Rietveld, *J. Appl. Crystallogr.* **2,** 65 (1969).
8. E. Prince, U. D. Tech. Note 1117 (F. J. Shorten, Ed.), pp. 8–9, National Bureau of Standards, Washington, D.C. (1980).
9. A. Santoro, R. J. Cava, D. W. Murphy, and R. S. Roth, "Neutron Scattering" (J. Faber, Ed.), N. 89, p. 162, AIP Conference Proceedings, New York (1982).
10. G. E. Bacon, *Acta Crystallogr. Sect. A* **28,** 357 (1972).
11. M. Horn, C. F. Schwerdtfeger, and E. P. Meagher, *Z. Kristallogr.* **136,** 273 (1972).
12. R. J. Cava, A. Santoro, D. W. Murphy, and S. Zahurak, *J. Solid State Chem.* **48,** 309 (1983).
13. S. Asbrink and A. Magneli, *Acta Crystallogr.* **12,** 575 (1959).
14. D. E. Cox, G. Shirane, P. A. Flinn, S. L. Ruby, and W. J. Takei, *Phys. Rev.* **132,** 1547 (1963).